

1 **Climatic variability during the last millennium in Western Iceland from lake sediment**
2 **records**

3

4 Naomi Holmes^a, Peter G. Langdon^{b*}, Chris J. Caseldine^c, Stefan Wastegård^d, Melanie J. Leng^{e,f}, Ian W.
5 Croudace^g and Siwan M. Davies^h

6

7 ^aDepartment of the Natural and Built Environment, Sheffield Hallam University, Sheffield, S1 1WB,
8 UK

9 ^bGeography and Environment, University of Southampton, Southampton, SO17 1BJ, UK

10 ^cGeography, Penryn Campus, University of Exeter, Penryn, Cornwall, TR10 9FE, UK

11 ^dDepartment of Physical Geography, Stockholm University, SE-106 91 Stockholm, Sweden

12 ^eCentre for Environmental Geochemistry, School of Geography, University of Nottingham,
13 Nottingham, NG7 2RD, UK

14 ^fNERC Isotope Geosciences Facilities, British Geological Survey, Keyworth, Nottingham, NG12 5GG,
15 UK

16 ^gOcean and Earth Science, University of Southampton, National Oceanography Centre Southampton,
17 European Way, Southampton, SO14 3ZH, UK

18 ^hDepartment of Geography, College of Science, Swansea University, Singleton Park, Swansea, SA2
19 8PP, UK

20 *Corresponding author

21

22

23 **Abstract**

24 The aim of this research was to create a decadal scale terrestrial quantitative palaeoclimate record
25 for NW Iceland from lake sediments for the last millennium. Geochemical, stable isotope and
26 chironomid reconstructions were obtained from a lake sequence constrained by tephra deposits on
27 the Snæfellsnes peninsula, W Iceland. Obtaining a quantitative record proved problematic, but the
28 qualitative chironomid record showed clear trends associated with past summer temperatures, and
29 the sedimentological records provided evidence for past changes in precipitation, mediated through
30 catchment soil inwash. When the full range of chronological uncertainty is considered, four clear
31 phases of climatic conditions were identified: (1) a relatively warm phase between AD 1020 - 1310;
32 (2) a relatively stable period between AD 1310 and AD 1510, cooler than the preceding period, but
33 still notably warmer than the second half of the millennium; (3) a consistent reduction of
34 temperatures between AD 1560 - 1810, with the coolest period between AD 1680-1810; (4) AD 1840
35 - 2000 has temperatures mainly warmer than in the preceding two centuries, with a rising trend and
36 increased variability from c. AD 1900 onwards. The reconstructions show clearly that the first half of
37 the millennium experienced warmer climatic conditions than the second half, with a return to the
38 warmer climate only occurring in the last c. 100 years. Much of the variability of the chironomid
39 record can be linked to changes in the North Atlantic Oscillation (NAO). The reconstructions
40 presented can track low frequency and long-term trends effectively and consistently but high
41 resolution and calibrated quantitative records remain more of a challenge – not just in finding
42 optimal sedimentary deposits, but also in finding the most reliable proxy. It is this that presents the
43 real challenge for Holocene climate reconstruction from this key area of the North Atlantic.

44

45

46 *Keywords*

47 *Iceland – palaeolimnology – chironomids– Little Ice Age – Medieval Climate Anomaly – North Atlantic*

48 *Oscillation*

49

50

51

52

53

54

55

56

57 Introduction

58 Understanding spatial variability in palaeoclimatic reconstruction relies heavily on high resolution
59 quantitative data provided from climate proxies. Because of the importance of the sensitivity of the
60 arctic and sub-arctic to climate change there have been attempts to derive such reconstructions for
61 the North Atlantic (Kaufman et al., 2009) and a number of sites in Iceland have been examined for
62 their palaeolimnological records to potentially be used for such reconstructions (Axford et al., 2009;
63 2011; Geirsdóttir et al., 2009a; Langdon et al., 2011; Larsen et al., 2011, 2012). Typically it has
64 proved problematic to calibrate Icelandic proxy records into a quantitative temperature record. For
65 example a biogenic silica (BSi) record for the last 2000 years from the Icelandic site Haukadalsvatn
66 has been shown to be a proxy for spring/summer conditions related to diatom productivity
67 (Geirsdóttir et al., 2009b), but it did not prove possible to calibrate this quantitatively. At other lakes
68 in Iceland attempts have been made to provide quantitative data utilising chironomid-inferred July
69 temperatures based on the Icelandic chironomid training set (Axford et al., 2007; Langdon et al.,
70 2008, Holmes et al., 2011), and a multi-decadal scale summer temperature record now exists for NW
71 Iceland since AD 1650 (Langdon et al., 2011). Longer records do exist, but at lower resolution
72 (centennial scale) and quantification has relied on DCA axis related temperature correlations (Axford
73 et al., 2009) or using a Norwegian chironomid training set (Caseldine et al., 2003).
74 Palaeolimnological approaches have therefore yet to provide consistent high-resolution quantitative
75 terrestrial temperature records for the later Holocene in Iceland. There are a number of potential
76 reasons for this:

- 77 (1) It is still unclear what sort of lake provides the best sediments for analysis in Iceland. Axford
78 et al. (2009) have highlighted difficulties with large, deep lakes, especially for chironomid
79 based temperature reconstruction approaches. Additionally, with any transfer function
80 approach, there may be problems associated with secondary gradients (Juggins 2013), and
81 hence caution is required in interpreting such reconstructions;
- 82 (2) Altitude may also be significant as the only Icelandic lake to produce chironomid based proxy
83 results that correlate well with instrumental data, Mýfluguvatn, lies at 435 m above sea level
84 (Langdon et al., 2011), and may well indicate that it is only at higher altitudes that climate
85 changes will be significant enough to register in the faunal or sedimentary records. If this is
86 the case then these lakes are likely to have relatively low sedimentation rates, and relatively
87 low concentrations of potential proxies;
- 88 (3) Post Settlement (~AD 874) human influences on catchments, particularly soil erosion
89 (McGovern et al., 2007), have been shown to affect chironomid assemblages within lakes

90 (Lawson et al., 2007). Careful site selection, limiting the effects of human settlements, is
91 important, particularly over the instrumental (calibration) period;

92 (4) There are as yet few proxies that have the potential to provide quantitative palaeoclimatic
93 data. % BSi has been interpreted as responding to local diatom productivity, which in turn is
94 a function of climate, especially the duration of the ice-free season and spring temperatures
95 (Geirsdóttir et al., 2009b; Striberger et al., 2012), but does not yet provide a quantitative
96 signal. Similarly at Haukadalsvatn Geirsdóttir et al. (2009b) have shown that the sediment
97 total organic carbon content (TOC) is strongly related to soil erosion and summer
98 temperatures, but again not yet quantified. Chironomid-based calibration models can be
99 used to provide chironomid-inferred temperature (C-IT) reconstructions (Langdon et al.,
100 2008; Axford et al., 2007, 2009; Holmes et al., 2011) although they have not yet been widely
101 tested at a variety of locations and lake types in Iceland;

102 (5) Chronology and sedimentation rate still play an important role in determining whether lake
103 sediments can provide high resolution, robust data. Radiocarbon dating has been found to
104 present problems in Iceland (Geirsdóttir et al., 2009b), ideally requiring a sound
105 tephrochronology for age-depth profiles, possibly with assistance from palaeomagnetism
106 (Ólafsdóttir et al., 2013).

107

108 Multiproxy, tephrochronologically constrained data presented here from Baulárvallavatn, studied as
109 part of the EU-funded MILLENNIUM project, attempt to address the issues raised above. Owing to
110 the location of Iceland in such an important position for the climate of the North Atlantic and the
111 development of high quality marine records that are now available for the region (e.g., Massé et al.,
112 2008; Ólafsdóttir et al., 2010; Sicre et al., 2011; Cunningham et al. 2013) it is important to determine
113 how best to provide the necessary terrestrial equivalent and the results from this study reveal both
114 the potential and problems of such work.

115

116 **Study Site**

117 Baulárvallavatn (64°54'N, 22°53'W) in western Iceland (Figure 1a) was selected after preliminary
118 examination of a range of lakes in the region to provide a high-resolution palaeoclimate record for
119 the last 1000 years. The site was chosen because it is located only 20 km from the meteorological
120 station at Stykkishólmur which has an observational record dating back to AD 1845, extended to AD
121 1823 using data from Reykjavík (available at <http://www.vedur.is>), providing a good opportunity to
122 validate the proxy record over the observational period. Lakes closer to the station were considered
123 to be more affected by human activity and to likely be less sensitive to temperature variations lying

124 close to sea level. Baulárvallavatn, located at 193 m above sea level, was considered more likely to
125 be temperature sensitive, whilst retaining a reasonable sedimentation rate. Additional site
126 description and data are detailed in Holmes et al. (2009).

127

128 **Materials and Methods**

129 *Fieldwork*

130 A bathymetric profiling of the lake (Figure 1b) was produced by traversing the lake in a boat with a
131 depth sounder and portable GPS. A 70 cm core (BAUL) was obtained from a water depth of 30 m
132 using a UWITEC corer. The core was not taken from the deepest part of the lake (46m) but was from
133 a relatively flat bottomed part of the lake (Figure 1b), as in the deeper areas the lake bottom shelved
134 steeply and potential problems exist with using the Icelandic temperature transfer function on deep
135 ($z_{\max} > 30\text{m}$) sites (Axford et al., 2009). The core was returned to the laboratory where it was stored
136 at 4 °C. Other replicate cores were taken from across the basin, and key stratigraphic changes and/or
137 specific measured parameters are reported below.

138

139 *Sediment geochemistry*

140 On return to the laboratory the core was split in half and analysed using the Itrax micro-XRF core
141 scanner (Croudace et al., 2006) at the British Ocean Sediment Core Research Facility (National
142 Oceanography Centre, Southampton). These analyses provided X-radiographic images and down-
143 core elemental compositional variations at a 200 μm resolution. The XRF data were acquired using a
144 Mo X-ray tube running at 30kV 30mA. A count time of 15 seconds per increment was used.

145

146 *Chronology*

147 Despite the well documented problems of radiocarbon dating in Icelandic lakes, primarily due to old
148 carbon entering the lake system through terrestrial and/or groundwater pathways, some pilot
149 radiocarbon analyses were attempted on BAUL. Due to a lack of terrestrial macrofossils within the
150 core five bulk sediment subsamples were sent to the Poznan Radiocarbon laboratory for dating, with
151 one level, 47-47.5 cm, also being analysed for the humic acid fraction. A water sample (taken in
152 2007) was also analysed for its radiocarbon content.

153

154 The uppermost samples were freeze dried and analysed for ^{137}Cs by gamma spectroscopy using a
155 well-type coaxial low background intrinsic germanium detector. ^{137}Cs was measured using the 660
156 keV gamma energy and counting was for 100 ksec for each sample. The efficiency function of the
157 detector was determined using an NPL (Teddington, UK) certified mixed gamma source.

158

159 Tephra analyses can be a useful addition to developing chronological models in Iceland (e.g. Boyle
160 1999; Caseldine et al., 2006), although relatively large volumes of background ash levels can make
161 identifying individual eruptions problematic. In western Iceland relatively few primary ashfalls have
162 been identified (Thordarsson and Höskuldsson, 2008), which is unsurprising given the prevailing
163 westerly winds and that all major volcanic centres, except Snæfellsjökull, are located to the east.
164 Following visual and x-ray inspection of the core, and XRF scanning a number of samples were
165 selected for tephra analyses (cf. Kylander et al., 2012). These samples were sieved (80 and 25 μm)
166 and processed using a heavy-liquid separation method (Turney, 1998) to isolate the 2.3-2.5 g/cm^3
167 and $>2.5 \text{ g}/\text{cm}^3$ fractions. Each fraction was prepared onto slides for geochemical analysis by
168 electron microprobe analysis (EPMA). A Cameca SX-100 microprobe housed at the University of
169 Edinburgh was used for this work and the operating conditions followed those outlined in Hayward
170 (2012). In order to derive a chronological model with estimated age uncertainties throughout the
171 core the chronological information (coring date, ^{137}Cs peak and tephra dates) were input into the R
172 package Bchron (Haslett and Parnell, 2008). Bchron (MCMC function, 100000 iterations) fits a
173 compound Poisson-gamma distribution to the increments between the dated levels; these are then
174 used to predict ages for depths through the core. The mean chronology was calculated and is the
175 chronology that is used to plot the downcore data from Baulárvallavatn. The full range of
176 chronological models (10000) provides us with chronological uncertainties for the whole core not
177 usually afforded when using historical tephrochronology.

178

179 *Magnetic susceptibility*

180 The magnetic susceptibility of discrete samples (0.5 cm freeze dried samples) was measured using a
181 Bartington MS2 Susceptibility system (Dearing, 1994). Both low (χ_{lf}) and high (χ_{hf}) frequency mass
182 magnetic susceptibility were measured, and percentage frequency dependent susceptibility ($\chi_{\text{fd}}\%$)
183 was calculated.

184

185 *$\delta^{13}\text{C}$, %TOC, and %TN*

186 Bulk sediment organic carbon isotope ratios ($\delta^{13}\text{C}_{\text{organic}}$), total organic carbon (%TOC) and total
187 nitrogen (%TN) were determined on decarbonated samples using a Carlo Erba Elemental Analyser
188 (NA 1500) attached to a VG Optima mass spectrometer and VG Triple Trap. $\delta^{13}\text{C}_{\text{organic}}$ values were
189 calculated to the VPDB scale using a within-laboratory standard (BROC) (replication precision of
190 $\pm 0.12\%$; 2σ). %TOC and %TN were determined with reference to an Acetanilide standard
191 (replication precision 0.16; 2σ). These values were used to calculate weight C/N ratios.

192

193 *Diatom and modern water stable isotopes*

194 Samples for $\delta^{18}\text{O}_{\text{diatom}}$ were prepared using a process of chemical digestion, differential settling,
195 sieving and heavy liquid separation loosely based on Morley et al. (2004). Sediment samples were
196 treated with 30% H_2O_2 at 90°C until reactions ceased (to remove organic material), before using 5%
197 HCl to eliminate any carbonates. Following differential settling, all samples were centrifuged in
198 sodium polytungstate ($3\text{Na}_2\text{WO}_4 \cdot 9\text{H}_2\text{O}$) (SPT) heavy liquid, resulting in the separation and
199 suspension of diatoms from the heavier detrital residue. The purified diatom samples were then
200 sieved at 10 μm and checked for purity using microscopy. Multiple cleans were required to ensure
201 that all tephra shards were removed. Purified diatom samples were analysed for $\delta^{18}\text{O}_{\text{diatom}}$ using the
202 step-wise fluorination method outlined in Leng and Sloane (2008). The outer hydrous layer of the
203 diatom, known to freely exchange isotopically with water (e.g. Juillet-Leclerc and Labeyrie, 1987),
204 was removed in a pre-fluorination stage using BrF_5 at low temperature. This was followed by a full
205 reaction at high temperature to liberate oxygen that was then converted to CO_2 (Clayton and
206 Mayeda, 1963) and measured for $\delta^{18}\text{O}_{\text{diatom}}$ using a MAT253 dual-inlet mass spectrometer. All $\delta^{18}\text{O}$
207 values were converted to the VSMOW scale using the within-run laboratory standard BFCmod, and
208 are reported here in per mil (‰). Replication precision for $\delta^{18}\text{O}$ is typically $\pm 0.3\text{‰}$

209

210 Oxygen isotope ($\delta^{18}\text{O}$) measurements on water samples were made using the CO_2 equilibration
211 method with an Isoprime 100 mass spectrometer plus Aquaprep device. Deuterium isotope (δD)
212 measurements were made using an online Cr reduction method with a EuroPyrOH-3110 system
213 coupled to a Micromass Isoprime mass spectrometer. Isotope measurements used internal
214 standards calibrated against the international standards VSMOW2 and VSLAP2. Replication
215 precisions are typically $\pm 0.05\text{‰}$ for $\delta^{18}\text{O}$ and $\pm 1.0\text{‰}$ for δD .

216

217 *Subfossil chironomids*

218 Samples were prepared for subfossil chironomid analysis using standard techniques (Brooks et al.,
219 2007) including ultrasound treatment (Lang et al., 2003). The head capsules were identified using
220 Hofmann (1971), Wiederholm (1983), Schmid (1993), Rieradevall and Brooks (2001) and Brooks et al.
221 (2007). The chironomid diagram was produced using C2 (Juggins, 2007). Principal components
222 analysis (PCA) was undertaken using Canoco (ter Braak and Smilauer, 2002) and both the Icelandic
223 chironomid-inferred July air temperature transfer function (Langdon et al., 2008) and a combined
224 Norwegian-Icelandic chironomid-inferred July air temperature transfer function (Holmes et al., 2011)
225 were applied to the downcore data using C2 (Juggins, 2007). Bchronproxplot (Parnell and Haslett,

226 2008) was used to produce inferred climate reconstructions showing the full range of chronological
227 uncertainty.

228

229

230 **Results**

231 *Sediment geochemistry*

232 The X-radiographs generated images revealing clear millimetric and sub-millimetric layering (Figure
233 2). The distinct dark bands correspond to denser mineralogical layers that most likely indicate ash
234 layers or in-wash events. The higher density of such layers may relate to composition and/or finer
235 grain size. The identification of relative density variations of layers at medium to high resolution
236 coupled with the elemental analytical capability permits the potential recognition of marker layers,
237 which were investigated further to try and identify well defined tephra layers (see below). The
238 elemental signatures of the layers seen implied that recognition is easiest with intermediate-acid
239 igneous compositions (co-variation in Si, K, Rb and Zr). Two tephras were identified, both from the X-
240 radiograph and clear peaks in K and Zr, towards the base of the core, at depths of 55-56 cm and 66-
241 67 cm (Figure 2).

242

243 Other elemental signatures and ratios can typically be used to help identify variations in clastic input.
244 For example, Si/Ti are typically used to reflect clastic input associated with grain size variations (e.g.
245 Chawchai et al, submitted), although other researchers have argued it can be a proxy for biological
246 silica (BSi) (Johnson et al. 2011; Liu et al. 2013). Si has multiple roles in geochemical processes, being
247 found in siliceous microfossils and mineral material. Given the large amount of mineral materials in
248 Icelandic lake sediments, notably from (often reworked) basalts and related igneous material, the
249 Itrax data was studied to see if we could see evidence for changes in clastic input, which may be
250 driven by changes in precipitation. Zr/Rb ratios were examined, as Rb is commonly associated with
251 clay, while Zr is enriched in coarse silts, hence high Zr/Rb reflect coarse particles (Schillereff et al.
252 2014). However, the dominant basaltic composition of sediment sources in the Baulárvallavatn
253 catchment makes the use of geochemical proxies for environmental/precipitation changes (e.g. Si/Ti,
254 Zr/Rb) difficult as the Itrax signals for Si and Rb are small (except where there is a contribution from
255 more evolved ash-rich layers of intermediate to silicic composition). So in the current context the
256 Itrax data (geochemistry and radiograph) aid the identification of tephras (especially intermediate-
257 silicic), but elemental profiles do not indicate any clear variations that correlate with other proxies
258 for environmental change.

259

260 *Chronology*

261 The ¹³⁷Cs analyses showed a clear peak in levels attributed to 1963 at 2.5 cm depth. Providing a
262 longer chronology for the sediment sequence proved to be problematic. The series of radiocarbon
263 dates showed no regular change through time with all dates providing values between 2600-2100
264 ¹⁴C yr BP (Table 1). A radiocarbon determination of modern lake water (sampled in 2007) showed
265 considerable input of old carbon from the eroding soils in the catchment and there is little reason to
266 believe that such an ageing effect will not have occurred consistently over the last millennium.

267

268 Eight samples were selected for tephra analyses. The two visible tephra layers (55-56 cm and 66-67
269 cm) were geochemically identified as the Landnám (AD871 ± 2; Grönvold et al., 1995) and Sn-1 (1780
270 ± 35 BP; Larsen et al., 2002) tephtras (Figure 3a). Both the basaltic and the rhyolitic component of the
271 Landnám tephra were present. Glass shards from the remaining tephra-rich horizons were
272 geochemically identified as deriving from the Hekla, Snæfellsjökull, Torfajökull, Katla and Veidivötn
273 volcanic systems (Table 2). The density fractions were dominated by silicic shards (SiO₂ >63%: 2.3-2.5
274 g/cm³) and basaltic shards (SiO₂ 45-52%: >2.5 g/cm³). Intermediate shards (53-62% SiO₂) were found
275 in both density fractions. The silicic samples were dominated by shards from Torfajökull (To) and
276 Snæfellsjökull (Sn). These are interpreted as reworked shards from the Landnám and Sn-1 eruptions
277 (and possibly Sn-2 and Sn-3; Jóhannesson et al., 1981) since no younger tephtras from these systems
278 are known (Haflidason et al 2000). Silicic shards from Katla (SILK) occur in some samples. These
279 shards are also interpreted as reworked and can either derive from the youngest silicic eruption of
280 Katla, SILK-YN which is dated to 1676 ± 12 BP or the older SILK-N4 (Larsen et al., 2001, Larsen and
281 Eiríksson 2008). These eruptions had lobes extending to the northwest and it is possible that some
282 shards may have reached western Iceland and the catchment of Baulárvallavatn. Intermediate and
283 silicic shards from Hekla occur in most samples, and are especially abundant at 10-11 and 23-24 cm.
284 However, given the abundance of reworked shards from other older silicic eruptions, a significant
285 part of the Hekla shards can be expected to be reworked, in particular the highly silicic shards (SiO₂
286 >65%). Basaltic tephra from all the main basaltic volcanic systems occur in the samples, i.e.
287 Grímsvötn, Veidivötn and Katla. However, the dominant basaltic component has high Al₂O₃ (c. 15-16
288 wt %) and K₂O (c. 0.8-1.2 wt %) content and has affinities to basaltic lavas from the Snæfellsnes
289 Volcanic Zone, mostly those of the Ljosufjoll system (Kokfelt et al, 2009; Steinthorsson et al. 1985
290 and unpublished data). It could, however, also originate from the older hyaloclastite formations in
291 the vicinity of the lake and be blown or washed in to the lake.

292

293 All analyses are listed in Table 2 and details can be found in the Supplementary Material. The tephra-
294 based age model assumes that some of the analysed tephra shards are primary and represent true
295 isochrons in the sediment. We are aware, however, that the majority of the shards are likely
296 reworked by catchment processes. For example, several of the shards with Hekla affinity could be
297 reworked from prehistoric eruptions which had a westward distribution, e.g. Hekla-B and Hekla-C
298 (Larsen and Eiriksson, 2008). Although each sample contained a mixture of shards thought to
299 originate from different volcanic centres, we pinpoint the specific volcanic eruption based on the
300 abundance of shards and the known dispersal patterns of historical eruptions in Iceland. For
301 example, two samples (3-4 cm and 14-15 cm) contain relatively large amounts of shards from
302 Veiðivötn, but despite these relatively high numbers, we are not aware of any historical eruptions
303 from this centre being dispersed towards northwest Iceland, and hence interpret them as reworked
304 shards from the basaltic part of the Landnám tephra. The samples at 3-4 cm contain a numbers of
305 basaltic grains from Katla. Tephra was dispersed widely from the eruption of Katla in 1918 including
306 one lobe reaching Snæfellsnes (Larsen et al., 2014) and we suggest that the shards in the 3-4 cm
307 sample derive from that eruption. The sample at 10-11 cm has abundant tephra from several
308 volcanic systems. Silicic shards from Hekla, however, are one of the most abundant components
309 within this sample and it is possible that some of these shards ($\text{SiO}_2 < 65\%$) derive from the relatively
310 large eruption in 1766. Tephra-fall was reported from north and northwest Iceland but the Hekla
311 1766 deposit has as yet, not been found on Snæfellsnes (cf. Larsen et al., 2014). Tephra from the
312 eruption of Katla in 1721 reached western Iceland (Larsen et al., 2014) and we suggest that the few
313 Katla shards in the 14-15 cm may relate to this event. The same sample also contains a reasonable
314 number of shards from the Hekla volcanic system which may be derived from Hekla-1693 event. The
315 Hekla-1693 tephra was carried towards the northwest and has recently been confirmed in lake sites
316 in the Western fjords (Langdon et al., 2011). The sample at 23-24 cm is more difficult to assign to a
317 certain eruption. More than half of the analyses suggest an origin in the Hekla system and indeed
318 several of the analyses show similarities with the Hekla 1510/Loch Portain B tephra, found in
319 Scotland and Ireland (Figure 3b; Dugmore et al., 1995; Pilcher et al., 1996). Reports from Iceland,
320 however, are scarce (Larsen et al., 2014) and indicate a main dispersal axis towards the southwest.
321 Nonetheless, given the good matches identified in Figure 3b, we use Hekla 1510 in our age model
322 (Table 2). Only a few analyses are available from 29-30 cm and the shards with Hekla affinity do not
323 allow a secure correlation with any of the historic eruptions of Hekla. It is possible, however, that the
324 Hekla 1341 eruption reached the area since a tephra fall was reported in west and northwest Iceland
325 at this time (Thorarinsson 1967). We are unable to pinpoint a volcanic eruption for sample 33-34 cm.
326

327 The tephra dates (Table 2) were used alongside the ^{137}Cs data and coring date to produce a
328 chronological model using Bchron, which is presented in Figure 4. Given the uncertainties
329 associated with which Hekla eruption might be represented by the samples at 23-24 cm and 29-30
330 cm (as noted above), three age models were developed, taking into account the maximum
331 uncertainties (i.e. oldest and youngest possible tephras for the less certain Hekla levels). The most
332 parsimonious model is shown in Figure 4, with Hekla 1510 assigned to 23-24 cm, and Hekla 1341
333 assigned to 29-30 cm. This approach allows the estimation of chronological uncertainty through the
334 core; chronological uncertainty is smaller closer to the tephra layers where the chronology is
335 constrained by the most confident tephra matches. There is a reasonably constant sedimentation
336 rate of approximately 0.05 cm yr^{-1} during the past 1000 years. Although beyond the main timescale
337 focus of this study it can be seen that prior to Settlement the sedimentation rate was lower (c. 0.02
338 cm yr^{-1}), as would be expected from other Icelandic lake sites.

339

340 *%TOC, C/N, organic carbon isotope composition and magnetic susceptibility data*

341 The %TOC, C/N, $\delta^{13}\text{C}$ and magnetic susceptibility data (Figure 5) show clear changes through the
342 record. Isolated spikes (low %TOC values at AD 870 and AD 1341) reflect the dominant input of
343 isolated tephra horizons from single eruptions; details also identified from the Itrax elemental data
344 (cf. Kylander et al., 2012). Apart from the effect of the Sn-1 tephra (c. AD 170) prior to Settlement
345 the sedimentary records are relatively uniform implying little variability in catchment dynamics
346 through time, with a $\delta^{13}\text{C}$ value around -26‰ , %TOC of around 3% and C/N of c. 9. After Settlement
347 all these proxies show significant variations with a trend to increasing %TOC, lower $\delta^{13}\text{C}$, reaching $<-$
348 27‰ at the surface, and C/N values of between 10 and 12, though these decrease to around 9.5 at
349 the surface. Changes are less apparent in the magnetic susceptibility record with greater variability
350 before the last millennium, but slightly higher low frequency susceptibility values following
351 Settlement. A short lived peak in frequency dependent susceptibility c. AD 1210 stands out, which
352 also corresponds with an increased peak in %TOC, C/N and increase in $\delta^{13}\text{C}$.

353

354 *Modern water and diatom stable isotope composition*

355 Waters for isotope analysis were sampled soon after ice out (April/May 2007), which likely reflects
356 winter precipitation, and also from the preceding summer, July 2006, to compare any seasonal
357 differences. The winter waters had lower $\delta^{18}\text{O}$ compared to summer, and Baulárvallavatn and the
358 other nearby lakes all plot along the global meteoric water line (GMWL) (Figure 6), indicating the
359 lake waters represent seasonal variation in precipitation and a sub-annual lake water residence time
360 (St Amour et al., 2010). Two of the lakes, Svínavatn and Saurarvatn, have summer isotope

361 compositions that define a local evaporation line (LEL). Both these lakes are smaller and shallower
362 than Baulárvallavatn, suggesting that these lakes evaporate in the summer but are recharged in the
363 winter.

364

365 The diatom $\delta^{18}\text{O}$ data (Figure 5f) cover the period AD 100-1300. No samples were analysed post-
366 AD1300 as the background tephra concentrations were too great, prohibiting clean preparations
367 from being obtained, despite several attempts. The data pre-AD 1200 vary between +28.4 to +32‰,
368 with a mean value of +29.7‰. A peak value of +32‰ is centred on AD 295, with low values (around
369 +29‰) centred pre-AD 200, and around AD 540, AD 930, and AD 1140. Post-AD 1200, there is a
370 short-lived increase to +40‰ around AD 1205 before a decrease to +26‰, the lowest value
371 measured in the core, c. AD 1295. The extreme high value of +40‰ was replicated in multiple
372 sample analyses and compared with spikes in other sedimentological proxies (Figure 5). The isotopic
373 composition of present day waters ($\delta^{18}\text{O}$, δD) was measured from Baulárvallavatn and nearby lakes
374 (Figure 6).

375

376 *Chironomid stratigraphy*

377 Forty six chironomid taxa were identified in the Baulárvallavatn core; the percentage diagram (Figure
378 7) shows selected taxa only. The chironomid assemblage is dominated by *Heterotrissocladius*
379 *grimshawi*-type (between 24-73%) with *Psectrocladius sordidellus*-type (2-32%), *Chironomus*
380 *anthracinus*-type (0-32%), *Paracladopelma* (0-18%), *Eukiefferiella* (0-17%) and *Micropsectra* (0-14%)
381 the next most abundant taxa. These taxa commonly occur in high levels in many other Icelandic
382 lakes (Langdon et al., 2008). The majority of the chironomid taxa present occur throughout the core
383 and although there are no major changes in terms of one taxon replacing another, there are some
384 clear trends and oscillations in certain taxa throughout the core. The base of the sequence is
385 dominated by relatively high abundances (although variable) of thermophilous taxa such as *C.*
386 *anthracinus*-type and *P. sordidellus*-type that lasts until the early 1300s. There is a noticeable change
387 in chironomid assemblage c. AD 1450-1520, with an increase in *Chaetocladius*. The period from late
388 AD 1500 to mid AD 1800 has a relative increase in *Diamesa*, which typically represent cooler
389 conditions. Head capsule concentration ranged between 19 and 187 head capsules g^{-1} , with the
390 peak concentration of 187 head capsules g^{-1} occurring at c. AD 1220.

391

392 *Chironomid-inferred temperature reconstructions*

393 The most commonly used method to produce a temperature reconstruction from downcore data is
394 to apply a transfer function developed using a modern surface sample training set (e.g., Caseldine et

395 al., 2006; Axford et al., 2007; Langdon et al., 2008; Gathorne-Hardy et al., 2009). The mean July air
396 temperature reconstruction produced by applying the Icelandic transfer function (Langdon et al.,
397 2008) to the Baulárvallavatn data (Figure 7) shows a range of reconstructed temperatures of 2.5 °C
398 (maximum = 9.7 °C; minimum= 7.2 °C) during the past 1000 years. The chironomid samples covering
399 the period 1961-1990 infer a mean July air temperature of 8.59 °C. When this is compared with the
400 modelled mean July air temperature of 9.62 °C from 1961-1990 (Björnsson et al. 2003) it is clear
401 there is an under-prediction of over 1 °C (just within the model RMSEP of 1.1 °C). A combined
402 Norwegian-Icelandic transfer function (Holmes et al., 2011) was also applied to the data (Figure 7),
403 as this model may produce more realistic temperature reconstruction (Holmes et al., 2011). The
404 results from this approach were similar to those produced using the Icelandic transfer function,
405 though the range of reconstructed temperatures was slightly smaller (2.2 °C). When compared to
406 the Stykkishólmur instrumental temperature data (corrected for altitude) both the chironomid-
407 inferred temperature reconstructions produce values which under-predict by between 0.5 °C and 1
408 °C. It should be remembered that the chronological uncertainty precludes validation of the
409 chironomid data against the instrumental data, and therefore only a visual comparison is used here.
410 It is clear from this approach that the trends and pattern of the C-IT reconstructions are not similar
411 to the instrumental data. Over the whole period studied both the chironomid-inferred temperature
412 reconstructions suggest that the second half of the millennium had higher temperatures, with the
413 warmest period occurring between c. AD 1600-1840 and the warmest temperature reached c. AD
414 1800. This is contrary to what is known about the climate of this time from other data sources; as a
415 result the chironomid-inferred temperature reconstructions are not interpreted any further (cf.
416 Axford et al., 2009) and possible reasons for this are discussed below.

417

418 *Ordination of the chironomid data*

419 Detrended correspondence analysis (DCA) revealed a gradient of 0.98 standard deviation units
420 resulting in the linear treatment of the data in further analyses. PCA was carried out and PCA axis 1
421 scores are shown in Figures 7 and 8. The PCA axis 1 scores show a remarkable similarity to other
422 palaeoclimatic proxy data covering the same time period (Figure 9) and have been interpreted as
423 providing a palaeoclimatic reconstruction with higher PCA axis 1 scores reflecting warmer
424 temperatures and lower PCA axis 1 scores reflecting cooler temperatures (see below for discussion).

425

426 Figure 8 was produced using Bchronproxypilot in Bchron (Haslett and Parnell, 2008) and shows the
427 PCA axis 1 scores plotted using a sample of 1000 chronologies (grey lines) produced for the core.
428 The PCA axis 1 scores are also plotted against the mean chronology (black line); using this, the

429 highest PCA axis 1 score occurred c. AD 1060 while the lowest score occurred c. AD 1780. It can be
430 seen, when taking into consideration chronological uncertainty, that the period c. AD 1000 to c. AD
431 1550 has higher PCA axis 1 scores (and therefore was warmer) than the period c. AD 1550 to AD
432 2006. Looking at the grey plots it seems that the latter period has more variability, though this is
433 possibly due to tighter chronological constraint during this time. It is also clear from this diagram
434 that using data such as these (e.g. non-varved, non-annually resolved data) to perform calibration
435 against instrumental data would be unwise, therefore this has not been attempted as part of this
436 study. A better chronologically constrained core would be needed in order to do this.

437

438 **Discussion**

439 *The sediment record and lake history*

440 By combining the %TOC, C/N, $\delta^{13}\text{C}$ and sedimentation rate results it is possible to infer the changing
441 nature of sedimentation into the lake over the last millennium. Prior to Settlement (~AD 874)
442 sedimentation was low at 0.02 cm yr^{-1} and %TOC reflects lake productivity as seen in C/N values
443 below 10 (algal material), and $\delta^{13}\text{C}$ around -26‰ (typical of aquatic plants, Figure 5). Following
444 Settlement the rate of sedimentation increased by a factor of 2.5 to 0.05 cm yr^{-1} , with a rapid
445 doubling in %TOC and a change in C/N to over 10 (suggesting a terrestrial component). From around
446 AD 1400 there was a further gradual rise in C/N peaking at the end of the 19th century, mirroring a
447 change in $\delta^{13}\text{C}$ to -27‰ (values typical of terrestrial plants). The %TOC, C/N and $\delta^{13}\text{C}$ records
448 correlate well (Figure 9). As %TOC increases, so does C/N, indicating that the increase in %TOC is
449 driven by in-wash of terrestrial organic matter (higher C/N than algae) and hence old soil carbon and
450 terrestrial plant fragments were likely continuously added to the lake system (cf. Axford et al., 2009;
451 Gathorne-Hardy et al., 2009; Geirsdóttir et al., 2009b). The lower $\delta^{13}\text{C}$ with increased %TOC
452 corroborates this interpretation (Langdon et al. 2010). The alternative explanation, of increasing
453 algal productivity, would have led to increases in $\delta^{13}\text{C}$ (not decreases), as algae preferentially utilise
454 ^{12}C (Meyers and Teranes, 2001). Interestingly, it is this latter relationship that Geirsdóttir et al.
455 (2009b) found at Haukadalsvatn, with an associated increase in BSi, suggesting that the lake had
456 undergone a phase of enhanced productivity, perhaps stimulated through the input of increased
457 organic matter.

458

459 The ability of quite large plant remains to be deposited across the lake can be observed during spring
460 melt when rivers in flood and small debris flows extend over the remaining ice cover. It seems likely
461 that isolated peaks in $\delta^{13}\text{C}$ could indicate extreme winter/spring flood or flow events that move
462 material directly onto ice over the deeper parts of the lake, as a suite of cores from across the lake

463 showed occasional lenses of poorly humified plant debris. The importance of redeposited C in the
464 lake, both as particulate and dissolved material is evident from the radiocarbon analyses. The lake
465 water currently has a radiocarbon age of almost 3500 years and this, coupled with redeposited plant
466 and/or soil remains from the catchment, gives the relatively uniform set of ages for the lake
467 sediment. Sufficient macrofossil remains for dating were not available from the selected core,
468 although in an adjacent core a date of 2120 ± 30 ^{14}C BP was obtained from moss remains near the
469 base of the core, a date that fits well with the depth and age of the tephra Sn-1 in the sampled core.
470 Nonetheless, given the evidence of increased erosion from the catchment there is no guarantee that
471 ages from terrestrial macrofossils will be contemporaneous between the date of inwash and the
472 material being transported.

473

474 The increased soil erosion through the last millennium at Baulárvallavatn (increase in %TOC etc.) is
475 most likely due to one, or both, of two processes. Settlements at lower altitudes typically introduced
476 sufficient grazing around the lake to initiate severe and persistent soil erosion (e.g. Simpson et al.,
477 2004; Lawson et al., 2007), and this is likely a background effect. Superimposed on this are changes
478 in climate, as cooler dry summers can reduce vegetation cover, enhancing aeolian erosion and
479 transport of organic matter into the lake (Geirsdóttir et al., 2009b). Increases in %TOC can thus be
480 interpreted as moving towards cooler summers, with dry windy winters, as exemplified by
481 Geirsdóttir et al. (2009b). Following this line of argument, it seems likely that significant shifts in the
482 $\delta^{13}\text{C}$ record, as at c. AD 1240 and AD 1550, may well represent a climate driven signal, with the
483 highest %TOC and C/N and the lowest $\delta^{13}\text{C}$ (outside the most recent sediments) being found around
484 AD 1750, a period interpreted as particularly cold (see later discussion) (Figure 9). The emerging
485 interpretation is thus of a lake subject to enhanced organic input derived from the surrounding
486 catchment over the last millennium, in contrast to preceding centuries, which most likely reflects in
487 part an anthropogenic signal, but crucially, a strong climate signal through increased erosion of a less
488 resilient surface soil.

489

490 *Climate variability of the last 1000 years*

491 The $\delta^{18}\text{O}_{\text{diatom}}$ record (Figures 5 and 9) is interpreted in terms of changes in seasonal precipitation
492 following the arguments outlined in Rosqvist et al. (2013), as Baulárvallavatn is a hydrologically open
493 lake (low residence time, non-evaporative). When cool Arctic air masses dominate, lake waters have
494 low $\delta^{18}\text{O}$, whereas higher $\delta^{18}\text{O}$ would result from southwesterly derived north Atlantic air masses
495 (GNIP database, 2014). Rosqvist et al. (2013) argue that for their $\delta^{18}\text{O}_{\text{diatom}}$ records from Sweden,
496 temperature impacts on the stable isotope record are likely negligible, as the summer temperature

497 changes over the last 1000 years are in the order of 1 °C (Esper et al., 2012). Given the net effect of
498 an increased condensation temperature is in the order of +0.5‰/°C (following Rosqvist et al., 2013),
499 and the amplitude of the $\delta^{18}\text{O}_{\text{diatom}}$ record is 3.6‰ (pre AD 1200), it is likely that temperature is not
500 the main driver of this isotopic signal, compared to changing source of precipitation. The relatively
501 high values around AD 300, AD 650 and from AD 950-1100 likely suggest summer precipitation
502 (south westerly sources) dominated compared to winter Arctic precipitation. Conversely, around AD
503 540, AD 930 and AD 1150, winter precipitation was likely relatively dominant. The sharp peak just
504 after AD 1200, with extremely enriched stable isotopes, can be explained as a period of high
505 evaporation, or higher summer rainfall (with higher $\delta^{18}\text{O}_{\text{diatom}}$) and lower winter rainfall (lower
506 $\delta^{18}\text{O}_{\text{diatom}}$). In the former scenario of higher evaporation the lake level may have dropped sufficiently
507 to cause the lake to become effectively closed, thus increasing $\delta^{18}\text{O}_{\text{diatom}}$ further by higher
508 evaporation (Leng and Marshall, 2004). The final sample in the $\delta^{18}\text{O}_{\text{diatom}}$ dataset, around AD 1300
509 has the lowest $\delta^{18}\text{O}_{\text{diatom}}$, and thus is indicative of a shift to relative dominance of winter
510 precipitation compared with summer.

511

512 The $\delta^{18}\text{O}_{\text{diatom}}$ data and interpretation of the sedimentological proxies fits well with the chironomid
513 response (Figure 9). However, it is clear that the transfer function results do not correspond well
514 with the sedimentological data, given they show increased warming between c. AD 1600-1850,
515 when the other proxies suggest enhanced cooling. This is likely related to the increased %TOC, which
516 typically is associated with increased productivity and warming temperatures (e.g. Velle et al., 2010).
517 However, this relationship between productivity and climate can decouple, as argued in Brooks et al.
518 (2012). It is decoupled in the Icelandic transfer function (Langdon et al., 2008), as %TOC plots
519 orthogonal to summer temperature. The Langdon et al. (2008) model includes many lowland lakes,
520 where relatively high levels of organic productivity are associated with warmer temperature lakes.
521 Nonetheless, the large increases in %TOC in Baulárvallavatn, which are likely associated with cooler
522 summers (*cf.* Geirsdóttir et al., 2009b), does seem to affect the transfer function performance in
523 relation to the presence of a strong secondary gradient (Juggins, 2013), and it is thus not surprising
524 that sensible quantitative results are not generated. There are a number of semi-terrestrial taxa
525 (e.g., *Chaetocladus*, *Limnophyes*, *Paraphaenocladus/Parametriocnemus* and *Pseudosmittia*) present
526 at various points in the Baulárvallavatn chironomid record which could support the suggestion of
527 increased catchment erosion due to cooler summers and drier winter conditions. These taxa are
528 present in low numbers in the Icelandic training set and have relatively warm temperature optima
529 (Langdon et al., 2008) and may be a factor contributing to the unreliable temperature reconstruction
530 produced using the Icelandic transfer function, while an ecological interpretation (supported by the

531 PCA analyses) supports the assertion that they are responding to temperature. Despite the problems
532 with transfer functions outlined by Juggins (2013), there is strong evidence that chironomids are
533 sensitive to summer temperatures in Iceland (Caseldine et al., 2003, 2006; Langdon et al., 2008,
534 2011; Holmes et al., 2011) and hence in *some* lakes provide a valid temperature reconstruction.
535 Axford et al. (2009) argued for a link with August temperatures through a calibration with the
536 Stykkishólmur temperature record based on a relatively small sample of 10 data points. These
537 analyses showed a stronger relationship with mean annual temperature (possibly acting via the
538 effect of ice thickness and melt-out date on chironomid growing season length and emergence
539 date), but August temperatures were reconstructed due to the known relationship between summer
540 air and water temperature and chironomids (Axford et al., 2009). It has not been possible to carry
541 out a similar calibration exercise here, due to chronological uncertainty in the upper sediments, but
542 the variability seen in this record, compared to other independent proxy data from both terrestrial
543 and marine sources (Figure 10), is strongly suggestive of a climate signal, as for instance is also
544 shown in the high altitude site at Mýfluguvatn (Langdon et al., 2011), where there is co-variation
545 between the C-IT and DCA reconstructions. Thus, although not providing a calibrated quantitative
546 record for Baulárvallavatn the PCA record does provide additional faunally-based climate evidence
547 for the last millennium and has a much stronger chronological control in terms of known
548 uncertainties, than at any other Icelandic site that covers the last 1000 years. Clear periods of long-
549 term trends can be identified within the last 1000 years within the chironomid and other records
550 (Figure 10; inferring climate (summer temperature) from the chironomid PCA analyses), and group
551 broadly into four main phases:

552

553 AD 1020-1310

554 By comparison with the mid- to late 20th century it seems likely that temperatures were slightly
555 warmer in general during this period. The highest temperatures were seen as an isolated peak
556 around AD 1060 with cooling to a clear trough between AD 1130 and AD 1180. The first half of the
557 13th century was warm, comparable to the end of the 20th century, before a second dip after AD
558 1260 reaching a minimum around AD 1300. In summary the mean values between AD 1020 and AD
559 1310 could be interpreted as warmer than the *overall* 20th century mean with two, possibly three
560 phases of decadal cooling centred on c. AD 1060-70, AD 1140-80 and AD 1270-1310.

561

562 AD 1310-1560

563 Values are relatively stable between AD 1310 and AD 1510, cooler than in the preceding period, but
564 still notably warmer than the second half of the millennium. The period ends though with a sharp

565 decline to the second lowest values in the record centred on AD 1535 before returning to values
566 seen in the rest of the period at c. AD 1555.

567

568 AD 1560-1810

569 From AD 1560 the PCA record suggests a consistent decline in temperatures to a minimum around
570 AD 1780 with the lowest temperatures in the record. There is no evidence of any even short-term
571 return to those temperatures preceding AD 1560, with the coldest phase being marked between AD
572 1680-1810.

573

574 AD 1810 – late 20th century

575 Apart from an early single peak around AD 1815 values are generally lower than before AD 1560,
576 although warmer than in the preceding two centuries. The trend from c. AD 1900 onwards is for
577 rising temperatures with variability between samples comparable to those throughout the record.
578 By the most recent sample, representing the end of the 20th century and the beginning of the 21st
579 century, values rise to those found almost a thousand years previously.

580

581 When the full range of chronological uncertainty is considered the four phases of climatic conditions
582 are still valid (Figure 8), and it is clear that the first half of the millennium experienced warmer
583 climatic conditions than the second half, though with a return to the warmer climate occurring in the
584 last c. 100 years. Comparison of existing records with other terrestrial data and especially offshore
585 data reveal broad scale agreements (Figure 10). Axford et al. (2011) showed significant correlations
586 across marine records around Iceland, and that sites in the west of Iceland (and offshore) relate
587 strongly to the Irminger Current and North Atlantic Drift over time (Ólafsdóttir et al., 2010). Regional
588 climatic variations across Iceland during the Holocene have been apparent from a number of studies,
589 especially for earlier in the Holocene (Caseldine et al., 2006; Axford et al., 2007), and Axford et al.
590 (2011) argue that sites in the north of Iceland may be relatively less coupled to the west, although
591 the nature of the seasonal drivers enhancing this variability over millennial timescales is not clear.
592 The Baulárvallavatn record reinforces some of the broader climate reconstructions for the last
593 millennium: peak warmth in the 11th century AD, persisting with decadal variability to the mid-13th
594 century, a period of cooling in the early 14th century with quite variable but not cold temperatures
595 until a sharp drop c. AD 1535 preceding a more steady decline in temperatures through the 17th and
596 18th centuries, leading to a minimum around AD 1780-1800. Temperatures begin to recover through
597 the 19th and into the 20th century eventually producing conditions comparable to those at the
598 beginning of the millennium (cf. Miller et al., 2012).

599

600 The decadal resolution of the chironomid data appears to clearly capture a low frequency signal with
601 multi-decadal variability superimposed on it and occasional rapid excursions. This low frequency
602 signal compares well with the Haukadalsvatn low frequency signal and as such appears to reflect the
603 orbitally driven decrease in summer insolation for this region (PAGES 2k Consortium, 2013). A clear
604 change is observed around the start of the 13th century, shown by the initiation of a new directional
605 trend in the chironomid PCA reconstruction, which correlates with a change in magnetic
606 susceptibility and sedimentary proxies around AD 1210. The reconstructed cooling c. AD 1270-1310
607 coincides with a period of decreased summer temperature and increased ice growth (AD 1275-1300)
608 in Arctic Canada (Miller et al., 2012), and the beginning of a period of increased varve thickness in
609 Hvítárvatn (Larsen et al. 2011), thought to be the result of climatic changes started by a period of
610 explosive volcanism and propagated by sea-ice and ocean feedbacks (Miller et al., 2012). Andrews et
611 al. (2009) observe a major change in marine climate variability at this time, and it could be
612 interpreted as marking the climate system reorganisation and initial decline into climates associated
613 with the Little Ice Age.

614

615 The variability of the chironomid PCA axis 1 scores can be investigated further. Some periods exist of
616 relatively stable conditions with variation around a mean value, while at other times there are
617 relatively rapid shifts in regime between these stable periods, and short term severe 'events' likely
618 to be of sub-decadal duration. In order to examine this further, the PCA reconstruction was
619 smoothed using a negative exponential smoother; the analyses used a polynomial regression and
620 weights were computed from the Gaussian density function (sampling proportion 0.1, polynomial
621 degree 1). To best understand the nature of the variability in the chironomid data, the residuals of
622 the smoothed PCA were analysed through rolling windows of 50 years, 100 years and 200 years. The
623 results of each rolling window test were similar, and the 100 year dataset have been plotted against
624 North Atlantic Oscillation (NAO) variability (Trouet et al. 2009) for the last 1000 years (Figure 11).
625 The chironomid record shows a centennial scale variability that is persistent throughout the whole of
626 the last millennium. This variability is based on the residuals, and so exists on top of the long-term
627 trends noted above. Comparison with the NAO reconstruction from Trouet et al. (2009) shows a
628 clear match between the records (within the errors of the age model), especially between AD 1400-
629 2000. Before this, the oscillations in the chironomids pervade, while the NAO index shows a period
630 of relatively less variability but was in a phase of enhanced dominant mode. Interestingly the
631 magnitude of the variability of the chironomids is relatively large, and increasing from AD 1000-
632 1650, but thereafter reduced in magnitude. The phase of positive NAO is linked to enhanced zonal

633 flow, with westerlies delivering warmer weather to continental Europe, with the storm track moving
634 further north and so Iceland is warmer but wetter in winter. In more negative phases of the NAO sea
635 ice builds up around Iceland so it is cooler but drier. A wetter winter will likely increase snowfall
636 around Baulárvallavatn, which would be melted off in warmer summers, influencing chironomid
637 populations which typically respond to summer temperatures. Thus, the controls of NAO on
638 Icelandic temperature seem to match the variability of the chironomid faunas on a multi-decadal to
639 centennial scale. Other links have been made between NAO and aquatic ecosystems (e.g. Straile,
640 2002; Blenckner et al. 2007), with the dominant argument being for a link through food-webs
641 primarily controlled by faster population growth of algae in warmer waters. The peaks and troughs
642 in NAO at the multi-decadal scale (i.e. warmer/cooler climate) clearly relate to enhanced variability
643 of chironomid communities, suggesting that as the food-web is altered through NAO driven
644 mechanisms, the chironomids also respond in terms of relatively high levels of internal trophic level
645 variability.

646

647 *Wider significance and broader issues*

648 Examination of the Baulárvallavatn record, especially in comparison with the other available
649 Icelandic terrestrial data (Figure 10), raises a number of issues concerning how best to derive the
650 desired quantitative high resolution terrestrial temperature record that is really needed to compare
651 with onshore and offshore records elsewhere. It seems likely that at present chironomid-based
652 temperature reconstructions provide the best opportunity for calibrated quantitative data but it is
653 not clear whether a transfer function or calibrated PCA/DCA approach offers the best route (e.g.,
654 Velle et al., 2010; Brooks et al., 2012; Juggins, 2013; Berntsson et al., 2014). For some lakes the C-IT
655 training set based methodology, however the training set is derived (Holmes et al., 2011), does not
656 appear to be able to reflect likely real temperature changes. Looking for variability in the
657 palaeorecord using PCA/DCA seems to be more appropriate, though it is reliant on accurate and
658 precise chronologies. Alternatively, in some lakes the secondary gradients may be too strong to rely
659 overly on transfer function derived C-IT (Berntsson et al., 2014). If it is assumed that such faunal
660 approaches are the optimal choice then the pressing need is to establish the types of lakes that are
661 best suited. It may be that smaller, higher lakes are more sensitive to temperature change (e.g.
662 Langdon et al. 2011), as they are relatively buffered against human impact. Low altitude, large and
663 deep lakes such as Haukadalsvatn (Geirsdóttir et al., 2009b) and Lögurinn (Striberger et al., 2012)
664 offer important opportunities for proxies such as BSi and %TOC but calibration to temperature may
665 prove difficult, as human activities are likely to impact these proxies, although in the latter case the
666 presence of a chironomid fauna may eventually prove to provide a suitable temperature record.

667 Smaller lakes at relatively low altitudes have been shown to provide sensitive C-IT reconstructions,
668 despite the possible influence of settlement (e.g. Holmes, 2008; Gathorne-Hardy et al. 2009). It
669 remains to be seen whether high productivity (hence relatively high sample resolution), air
670 temperature sensitive lakes can be found at high enough altitudes to meet the necessary criteria. As
671 such the approach followed at Baulárvallavatn offers a promising opportunity for further
672 development at sites with comparable or better dating control, and for which a well developed
673 quantitative recent record would provide the sort of robust calibration required to produce a high
674 quality temperature reconstruction. The challenge remains to produce the sort of high resolution
675 calibrated data set for temperature that both offshore records and modelling studies merit but it is
676 only by the detailed analysis of sites considered potentially suitable that the most valuable records
677 will be discovered.

678

679

680 **Acknowledgements**

681 We would like to thank Gareth Thompson for help in the field and with preparing the diatom stable
682 isotope samples and running the sedimentological analyses. Hilary Sloane, Carol Arrowsmith and
683 Chris Kendrick are thanked for running the stable isotope analysis. We thank Tomasz Goslar for
684 discussion with the interpretation of radiocarbon dates. Andrew Parnell is thanked for his help with
685 the R package Bchron, particularly Bchronproxypplot. Helen Ward and Gareth James are thanked for
686 preparing the tephra samples for microprobe analysis. Chris Hayward at the Tephra Analytical Unit,
687 University of Edinburgh is thanked for help with tephra analyses. We are very grateful to Sigurður
688 Steinþórsson for his unpublished analyses on the Ljósufjöll system from the geochemical data base
689 at Science Institute, analyst Niels Oskarsson. The Southampton Cartographic unit is thanked for
690 preparing the figures.

691

692 **Funding**

693 The work described in this manuscript was undertaken through the MILLENNIUM project, which
694 focused on better understanding the European climate of the last Millennium. The project was
695 funded by the EU through FP6. We thank the funders, but also the project PI, Danny McCarroll, as
696 well as the WP3 leader Sheila Hicks, plus all colleagues who worked under the Millennium project for
697 stimulating and fruitful scientific discussion.

698

699 **References**

- 700 Andrews JT, Darby D, Eberle D et al. (2009) A robust, multisite Holocene history of drift ice off
701 northern Iceland: implications for North Atlantic climate. *The Holocene* 19: 71-77.
- 702 Axford Y, Miller GH, Geirsdóttir, Á et al. (2007) Holocene temperature history of northern Iceland
703 inferred from subfossil midges. *Quaternary Science Reviews* 26: 3344-3358.
- 704 Axford Y, Geirsdóttir Á, Miller GH et al. (2009) Climate of the Little Ice Age and the past 2000 years in
705 northeast Iceland inferred from chironomids and other lake sediment proxies. *Journal of*
706 *Paleolimnology* 41: 7-24.
- 707 Axford Y, Andresen CS, Andrews JT et al. (2011) Do paleoclimate proxies agree? A test comparing 19
708 late Holocene climate and sea-ice reconstructions from Icelandic marine and lake sediments.
709 *Journal of Quaternary Science* 26: 645-656.
- 710 Berntsson A, Rosqvist GC and Velle G (2014) Late-Holocene temperature and precipitation changes
711 in Vindelfjällen, mid-western Swedish Lapland, inferred from chironomid and geochemical data. *The*
712 *Holocene* 24: 78-92.
- 713 Björnsson H (2003) *The annual cycle of temperature in Iceland: the 1961–1990 average*. Technical
714 Report, Icelandic Meteorology Office.
- 715 Boyle JE (1999) Variability of tephra in lake sediments, Svinavatn, Iceland. *Global and Planetary*
716 *Change* 435: 129-149.
- 717 Blenckner T, Adrian R, Livingstone DM et al. (2007) Large-scale climatic signatures in lakes across
718 Europe: a meta-analysis. *Global Change Biology* 13: 1314-1326.
- 719 Brooks SJ, Langdon PG and Heiri O (2007) *The Identification and Use of Palaeartic Chironomidae*
720 *Larvae in Palaeoecology*. QRA Technical Guide No. 10. Quaternary Research Association, London.
- 721 Brooks SJ, Axford Y, Heiri O et al. (2012) Chironomids can be reliable proxies for Holocene
722 temperatures: A comment on Velle et al. (2010). *The Holocene* 22: 1495-1500.
- 723 Caseldine CJ, Geirsdóttir Á and Langdon PG (2003) Efstadalsvatn – a multi-proxy study of a Holocene
724 lacustrine sequence from NW Iceland. *Journal of Paleolimnology* 30: 55-73.
- 725 Caseldine CJ, Langdon PG and Holmes N (2006) Early Holocene climate variability and the timing and
726 extent of the Holocene thermal maximum (HTM) in northern Iceland. *Quaternary Science Reviews*
727 25: 2314-2331.
- 728 Chawchai S, Kylander M, Chabangborn A, et al. (submitted) An example of commonly used XRF core
729 scanning based proxies for organic rich lake sediments and peat. *The Holocene*
- 730 Clayton RN and Mayeda TK (1963) The use of bromine pentafluoride in the extraction of oxygen
731 from oxides and silicates for isotopic analysis. *Geochimica et Cosmochimica Acta* 27: 43-52.

732 Croudace I, Rindby A and Rothwell R (2006) ITRAX: description and evaluation of a new multi
733 function X-ray core scanner. In: Rothwell RG (ed) *New techniques in sediment core analysis:*
734 *Geological Society London Special Publication 267*, pp. 51–63.

735 Cunningham L, Austin WEN, Knudsen KL et al. (2013) Reconstructions of surface ocean conditions
736 from the northeast Atlantic and Nordic seas during the last millennium. *The Holocene* 23: 921-935.

737 Dearing JA (1994) *Environmental Magnetic Susceptibility*. Chi Publishing, Kenilworth.

738 Dugmore AJ, Larsen G, Newton AJ (1995) Seven tephra isochrones in Scotland. *The Holocene* 5: 257–
739 266.

740 Esper J, Büntgen U, Timonen M et al. (2012) Variability and Extremes of Northern Scandinavian
741 summer temperatures over the Past Two Millennia. *Global and Planetary Change* 88-89: 1-9.

742 Gathorne-Hardy FJ, Erlendsson E, Langdon PG et al. (2009) Lake sediment evidence for late-Holocene
743 climate change and landscape erosion in western Iceland. *Journal of Paleolimnology* 42: 413–426.

744 Geirsdóttir Á, Miller GH, Axford A et al. (2009a) Holocene and latest Pleistocene climate and glacier
745 fluctuations in Iceland. *Quaternary Science Reviews* 28: 2107-2118.

746 Geirsdóttir Á, Miller GH, Thordarson T et al. (2009b) A 2000 year record of climate variations
747 reconstructed from Haukadalsvatn, West Iceland. *Journal of Paleolimnology* 41: 95 115.

748 Grönvold K, Óskarsson K, Johnsen SJ et al. (1995) Tephra layers from Iceland in the Greenland GRIP
749 ice core correlated with oceanic and land sediments. *Earth and Planetary Science Letters* 135: 149–
750 155.

751 Gudmundsdóttir, ER, Larsen, G, Eiríksson, J (2012) Tephra stratigraphy of the North Icelandic shelf:
752 extending tephrochronology into marine sediment off North Iceland. *Boreas* 41, 719-734.

753 Haslett J and Parnell AC (2008) A simple monotone process with application to radiocarbon-dated
754 depth chronologies. *Journal of the Royal Statistical Society: Series C (Applied Statistics)* 57: 399-418.

755 Hayward CL (2012) High Spatial Resolution Electron Probe Microanalysis of Tephtras and Melt
756 Inclusions without beam-induced chemical modification. *The Holocene* 22: 119-125.

757 Hofmann W (1971) Zur Taxonomie und Palökologie subfossiler Chironomiden (Dipt.) in
758 Seesedimenten. *Ergebnisse der Limnologie, Archiv für Hydrobiologie Beiheft (International*
759 *Vereinigung für theoretische und angewandte Limnologie, Stuttgart)* 6: 1–50.

760 Holmes N (2008) Validation of chironomid-inferred temperature reconstructions in Iceland: the
761 potential for reconstructing quantitative changes in Holocene climate. *Geographica Helvetica* 63: 4-
762 14.

763 Holmes N, Langdon PG and Caseldine CJ (2009) Subfossil chironomid variability in surface sediment
764 samples from Icelandic lakes: implications for the development and use of training sets. *Journal of*
765 *Paleolimnology* 42: 281-295.

766 Holmes N, Langdon PG, Caseldine CJ et al. (2011) Merging chironomid training sets: implications for
767 palaeoclimate reconstruction. *Quaternary Science Reviews* 30: 2793-2804.

768 Jóhannesson H, Flores R and Jónsson J (1981) A short account on the Holocene tephrochronology of
769 the Snæfellsjökull volcano, Western Iceland. *Jökull* 31: 23-30.

770 Johnson TC, Brown ET and Shi J (2011) Biogenic silica deposition in Lake Malawi, East Africa over the
771 past 150,000 years. *Palaeogeography, Palaeoclimatology, Palaeoecology* 303: 103-109.

772 Juggins S (2007) *C2 User guide. Software for ecological and palaeoecological data analysis and*
773 *visualisation*. University of Newcastle, UK.

774 Juggins S (2013) Quantitative reconstructions in palaeolimnology: new paradigm or sick science?
775 *Quaternary Science Reviews* 64: 20-32.

776 Juillet-Leclerc A. and Labeyrie L (1987) Temperature dependence of the oxygen isotopic
777 fractionation between diatom silica and water. *Earth and Planetary Science Letters* 84: 69-74.

778 Kaufman DS, Schneider DP, McKay NP et al. (2009) Recent Warming Reverses Long-Term Arctic
779 Cooling. *Science* 325: 1236-1239.

780 Kokfelt TF, Hoernle K, Lundstrom C et al. (2009) Time-scales for magmatic differentiation at the
781 Snæfellsjökull central volcano, western Iceland: Constraints from U-Th-Pa-Ra disequilibria in post-
782 glacial lavas. *Geochimica et Cosmochimica Acta* 73: 1120-1144.

783 Kylander ME, Lind EM, Wastegård S et al. (2012) Recommendations for using XRF core scanning as a
784 tool in tephrochronology. *The Holocene* 22: 371-375.

785 Lang B, Bedford AP, Richardson N et al. (2003) The use of ultra-sound in the preparation of
786 carbonate and clay sediments for chironomid analysis. *Journal of Paleolimnology* 30: 451-460.

787 Langdon PG, Holmes N and Caseldine CJ (2008) Environmental controls on modern chironomid
788 faunas from NW Iceland and implications for reconstructing climate change. *Journal of*
789 *Paleolimnology* 40: 273-293

790 Langdon PG, Leng MJ, Holmes N et al. (2010) Lacustrine evidence of early-Holocene environmental
791 changes in northern Iceland: a multiproxy palaeoecology and stable isotope study. *The Holocene* 20:
792 205-214.

793 Langdon PG, Caseldine CJ, Croudace IW et al. (2011) A chironomid-based reconstruction of summer
794 temperatures in NW Iceland since AD 1650. *Quaternary Research* 75: 451-460.

795 Larsen G, Newton A, Dugmore A et al. (2001) Geochemistry, dispersal, volumes and chronology of
796 Holocene silicic tephra layers from the Katla volcanic system, Iceland. *Journal of Quaternary Science*
797 16: 119-132.

798 Larsen G, Eiríksson J, Knudsen K et al. (2002) Correlation of Late Holocene terrestrial and marine
799 tephra markers, north Iceland: implications for reservoir age changes. *Polar Research* 21: 283-290.

800 Larsen G and Eiríksson J (2008) Late Quaternary terrestrial tephrochronology of Iceland – frequency
801 of explosive eruptions, type and volume of tephra deposits. *Journal of Quaternary Science* 23: 109-
802 120.

803 Larsen G, Eiríksson J and Gudmundsdóttir ER (2014) Last millennium dispersal of air-fall tephra and
804 ocean-rafted pumice towards the north Icelandic shelf and the Nordic seas. In Austin WEN, Abbott
805 PM, Davies SM et al. (eds) *Marine tephrochronology*. Geological Society of London, Special
806 Publications 398: 113-140

807 Larsen DJ, Miller GH, Geirsdóttir Á et al. (2011) A 3000-year varved record of glacier activity and
808 climate change from the proglacial lake Hvítárvatn, Iceland. *Quaternary Science Reviews* 30: 2715-
809 2731.

810 Larsen DJ, Miller GH, Geirsdóttir Á et al. (2012) Non-linear Holocene climate evolution in the North
811 Atlantic: a high-resolution, multi-proxy record of glacier activity and environmental change from
812 Hvítárvatn, central Iceland. *Quaternary Science Reviews* 39: 14-25.

813 Lawson IT, Gathorne-Hardy FJ, Church MJ et al. (2007) Environmental impacts of the Norse
814 settlement: palaeoenvironmental data from Myvatnssveit, northern Iceland. *Boreas* 36: 1-19.

815 Leng MJ and Marshall JD (2004) Palaeoclimate interpretation of stable isotope data from lake
816 sediment archives. *Quaternary Science Reviews* 23: 811-831.

817 Leng MJ and Sloane HJ (2008) Combined oxygen and silicon isotope analysis of biogenic silica.
818 *Journal of Quaternary Science* 23: 313-319.

819 Liu X, Colman SM, Brown ET et al. (2013) Estimation of carbonate, total organic carbon, and biogenic
820 silica content by FTIR and XRF techniques in lacustrine sediments. *Journal of Paleolimnology* 50: 387-
821 398.

822 Massé G, Rowland SJ, Sicre M-A et al. (2008) Abrupt climate changes for Iceland during the last
823 millennium: evidence from high resolution sea ice reconstructions. *Earth and Planetary Science*
824 *Letters* 269: 565-569.

825 McGovern TH, Vésteinsson O, Friðriksson A et al. (2007) Landscapes of settlement in northern
826 Iceland: historical ecology of human impact and climate fluctuation on the millennial scale.
827 *American Anthropologist* 109: 27-51.

828 Meyers PA and Teranes JL (2001) Sediment organic matter. In Last WM and Smol JP (eds) *Tracking*
829 *environmental change using lake sediments. Volume 2: physical and geochemical techniques*. Kluwer
830 Academic Publishers, pp. 239–69.

831 Miller GH, Geirsdóttir Á, Zhong Y et al. (2012) Abrupt onset of the Little Ice Age triggered by
832 volcanism and sustained by sea-ice /ocean feedbacks. *Geophysical Research Letters* 39: L02708.

833 Morley DW, Leng MJ, Mackay AW et al. (2004) Cleaning of lake sediment samples for diatom oxygen
834 isotope analysis. *Journal of Paleolimnology* 31: 391-401.

835 Ólafsdóttir S, Jennings AE, Geirsdóttir Á et al. (2010) Holocene variability of the North Atlantic
836 Irminger Current on the south- and northwest shelf of Iceland. *Marine Micropaleontology* 77: 101-
837 118.

838 Ólafsdóttir S, Geirsdóttir Á, Miller GH et al. (2013) Synchronizing Holocene lacustrine and marine
839 sediment records using paleomagnetic secular variation. *Geology* 41: 535-538.

840 PAGES 2k Consortium (2013) Continental-scale temperature variability during the past two
841 millennia. *Nature Geoscience* 6: 339-346.

842 Pilcher JR, Hall VA and McCormac FG (1996) An outline tephrochronology for the Holocene of the
843 north of Ireland. *Journal of Quaternary Science* 11: 485–494.

844 Rieradevall M and Brooks SJ (2001) An identification guide to subfossil Tanypodinae larvae (Insecta:
845 Diptera: Chironomidae) based on cephalic setation. *Journal of Paleolimnology* 25: 81-99.

846 Rosqvist GC, Leng MJ, Goslar T et al. (2013) Shifts in precipitation during the last millennium in
847 northern Scandinavia from lacustrine isotope records. *Quaternary Science Reviews* 66: 22-34.

848 Schillereff DN, Chiverrell RC, Macdonald N et al. (2014) Flood stratigraphies in lake sediments: A
849 review. *Earth-Science Reviews* 135: 17-37.

850 Schmid PE (1993) A key to the larval Chironomidae and their instars from Austrian Danube region
851 streams and rivers. Part 1: Diamesinae, Prodiamesinae and Orthocladiinae. *Wasser und Abwasser*
852 *Supplementband* 3/93: 1-513.

853 Sicre M-A, Hall IR, Mignot J et al. (2011) Sea surface temperature variability in the subpolar Atlantic
854 over the last two millennia. *Paleoceanography* 26: PA4218.

855 Simpson I, Gudmundsson G, Thomson AM et al. (2004) Assessing the role of winter grazing in historic
856 land degradation, Myvatnssveit, northeast Iceland. *Geoarchaeology* 19: 471-502.

857 St. Amour NA, Hammarlund D, Edwards TWD et al. (2010) New insights into Holocene atmospheric
858 circulation dynamics in central Scandinavia inferred from oxygen-isotope records of lake-sediment
859 cellulose. *Boreas* 39: 770-782.

860 Straile D (2002) North Atlantic Oscillation synchronizes food-web interactions in central European
861 Lakes. *Proceedings of the Royal Society of London, Series B* 269: 391-395.

862 Striberger J, Björck S, Holmgren S et al. (2012) The sediments of Lake Lögurinn – A unique proxy
863 record of Holocene glacial meltwater variability in eastern Iceland. *Quaternary Science Reviews* 38:
864 76-88.

865 ter Braak CJF and Šmilauer P (2002) *CANOCO Reference Manual and CanoDraw for Windows User's*
866 *Guide: Software for Canonical Community Ordination (version 4.5)*. Microcomputer Power, New
867 York.

868 Thorarinsson, S. (1967) The eruptions of Hekla in historical times. The eruption of Hekla 1947-1948.
869 Volume 1. *Societas Scientiarum Islandica*: 1-183.

870 Thordarsson T and Höskuldsson Á (2008) Postglacial volcanism on Iceland. *Jökull* 58: 197-228.

871 Trouet V, Esper J, Graham NE et al. (2009) Persistent positive North Atlantic oscillation mode
872 dominated the Medieval Climate Anomaly. *Science* 324: 78-80.

873 Turney CSM (1998) Extraction of rhyolitic component of Vedde microtephra from minerogenic lake
874 sediments. *Journal of Paleolimnology* 19: 199-206.

875 Velle G, Brodersen KP, Birks HJB et al. (2010) Midges as quantitative temperature indicator species:
876 Lessons for palaeoecology. *The Holocene* 20: 989-1002.

877 Wiederholm T (ed) (1983) Chironomidae of the Holarctic region. Keys and diagnoses. Part I. Larvae.
878 *Entomologica Scandinavica Supplement* 19: 1-457.

879

880 **List of Figures**

881 Figure 1: Location map of Baulárvallavatn (1a) and bathymetry, showing the coring location (1b).

882

883 Figure 2: X-radiograph and Itrax data. All elemental data are divided by the counts (kcps) and the
884 relative smoothing of the data are shown. The geochemical data do not reveal any clear variations
885 that can be linked to climate effects owing to the largely monolithic composition of catchment
886 material (weathered basalt). They are successful, however, in identifying likely ash horizons, as
887 shown by changes in the X-radiograph and associated oscillations in associated elements. Note the
888 large spikes in K towards the base of the sequence, which represent the Landnám and Sn-1 tephras
889 (see Table 2).

890

891 Figure 3: (a) Landnam vs SN-1 tephra plots; (b) Baulárvallavatn 23-24 cm (Hekla geochemistry) vs
892 Hekla 1510 and Loch Portain B.

893

894 Figure 4: Chronological model produced in Bchron. Coring date, ^{137}Cs (1963) date and tephra dates
895 (Table 2) were input. The plot shows the mean chronology and the 95% confidence limits (grey
896 shaded areas).

897

898 Figure 5: Sedimentological and isotope data. a) sediment %TOC; b) sediment $\delta^{13}\text{C}$; c) sediment C/N;
899 d) low frequency magnetic susceptibility; e) frequency dependent susceptibility; f) diatom $\delta^{18}\text{O}$.

900

901 Figure 6: Modern day isotopic composition of Baulárvallavatn and nearby lakes. The black filled
902 circles represent a range of samples taken in April/May 2007 (end of winter) from lakes on the
903 Snæfellsnes peninsula. Catchment sampling locations included lake inflows and outflows, snow beds
904 and peat water inflows. The black filled squares are lake waters from Baulárvallavatn and Svínavatn,
905 sampled in April 2006. The open diamonds reflect lake water samples taken in July 2007 (summer),
906 and show that while most lakes plot on or near to the GMWL, two lakes (Saurarvatn and Svínavatn)
907 plot away from the GMWL, suggesting they can be relatively evaporative in the summer.
908 Baulárvallavatn summer water samples plot on the GMWL.

909

910 Figure 7: Baulárvallavatn chironomid percentage data (selected taxa); Chironomid-inferred
911 temperature reconstructions, and PCA axis 1 scores.

912

913 Figure 8: Chironomid PCA axis 1 score reconstruction. Reconstruction using mean chronology is in
914 black. Reconstructions using 1000 sample chronologies are in grey.

915

916 Figure 9: Composite diagram, comparing the chironomid results (PCA axis 1 reconstruction and %
917 head capsule concentration) against the organics proxies from BAUL (%TOC, $\delta^{13}\text{C}$ and C/N) and the
918 diatom $\delta^{18}\text{O}$.

919

920 Figure 10: Composite diagram, showing chironomid results (PCA axis 1 reconstructions) against
921 selected terrestrial and marine proxies from Iceland including Stora Viðarvatn chironomid inferred
922 summer temperature (Axford et al. 2009), Haukadalsvatn BSi (Geirsdottir et al. 2009b), Hvítarvatn
923 ice thickness (Larsen et al. 2011), and offshore alkenone water temperatures (Sicre et al. 2011).

924

925 Figure 11: Comparison of chironomid variability against NAO over the last 1000 years.

926

927 **List of Tables**

928

929 Table 1. Radiocarbon determinations from the BAUL sequence.

930

931 Table 2. Details of the tephra found in each depth layer investigated. The different volcanic centres
932 are represented by Ka (Katla), Ve (Veiðivötn), Gr (Grímsvötn), Sn (Snæfellsnes) To (Torfajökull)
933 and Hk (Hekla). The numbers in parentheses after each eruption centre relate to the number of
934 shards identified from that centre according to the major element results (see Sup. Material). The
935 tephra in the right hand column represents the most likely eruption ascribed to each depth
936 layer, as discussed in the text. Note, for the 14-15 cm layer, both ages are used in the generation
937 of the age model (Figure 4).

938

939

940 **Supplementary Material**

941 Excel spreadsheet with detailed geochemical data from each tephra shard analysed under EMPA
942 from the BAUL sequence.

Fig 1

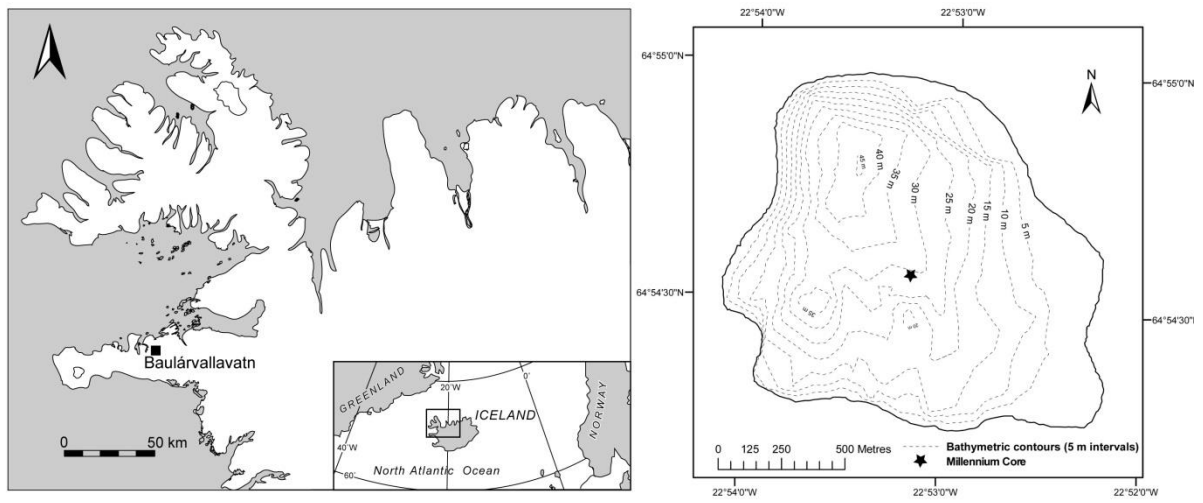
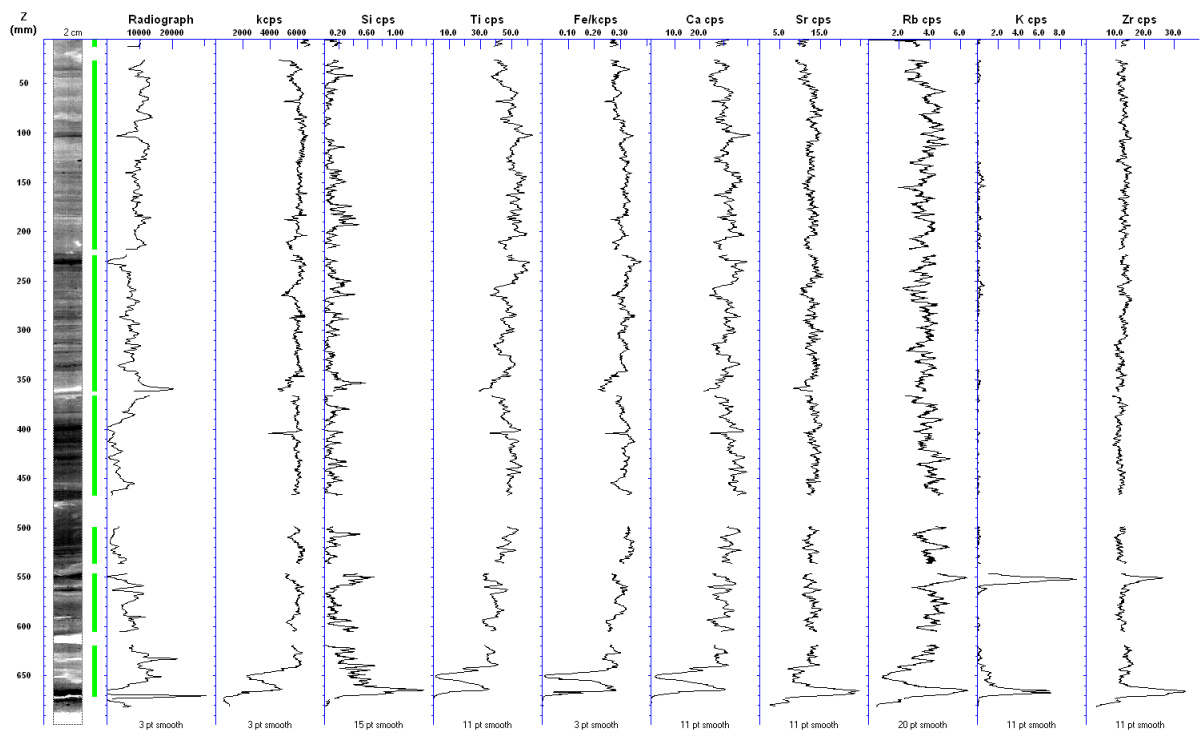


Fig 2



Core: BAUIAR-Da	Section: 1 FILM	User: PLANGDON4	Date: 04/09/2006 - Itrax-PLDT V2.69
X-Ray tube: Mo target	Line camera signal: 38717 at 25 ms	Filename: BAUIAR-Da-1 FILM	Data produced by the NDC Itrax
XRF Conditions	30 kV 30 mA	Step Size: 200 microns	Count time: 15 seconds/increment
X-radiograph Conditions	45 kV 40 mA	Step Size: 200 microns	Dwell time: 400 ms/increment

Fig 3

FIG X

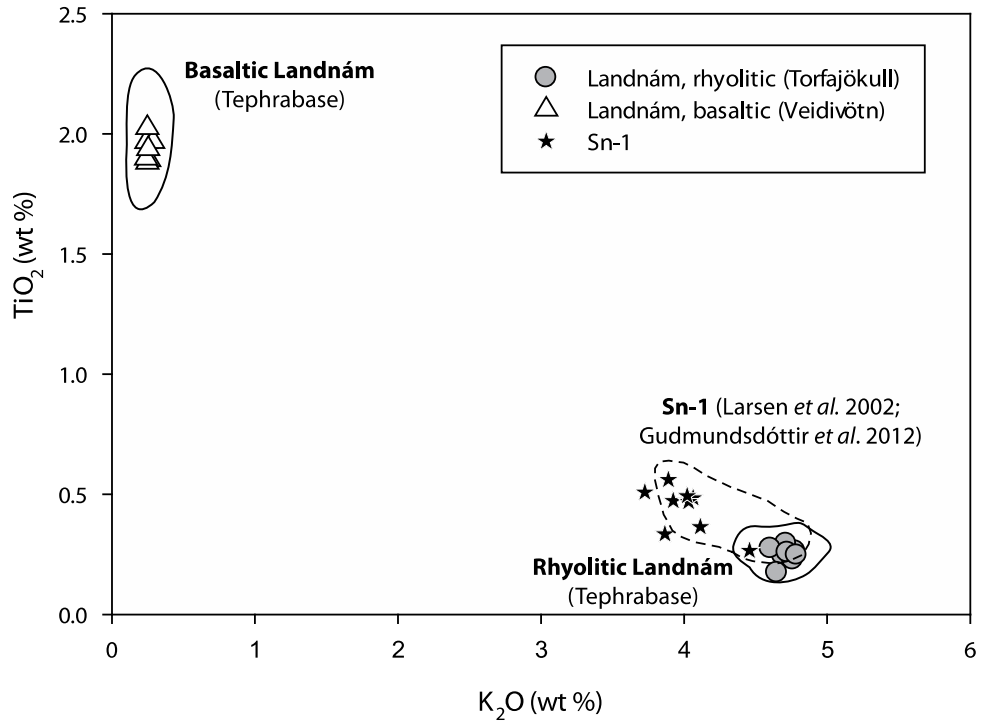


FIG Y

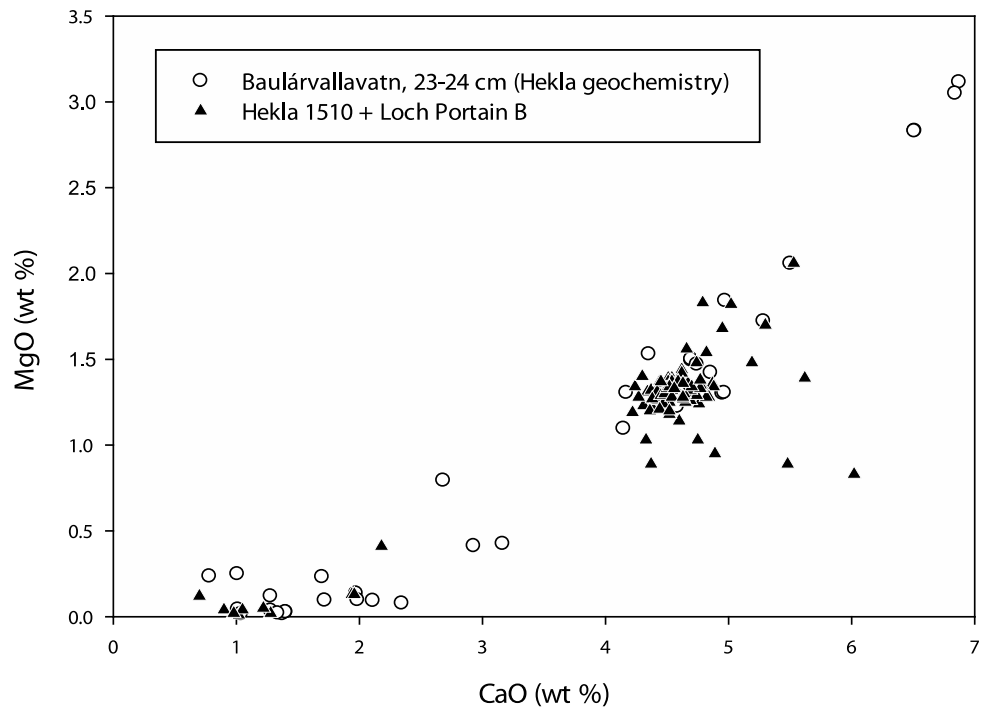


Fig 4

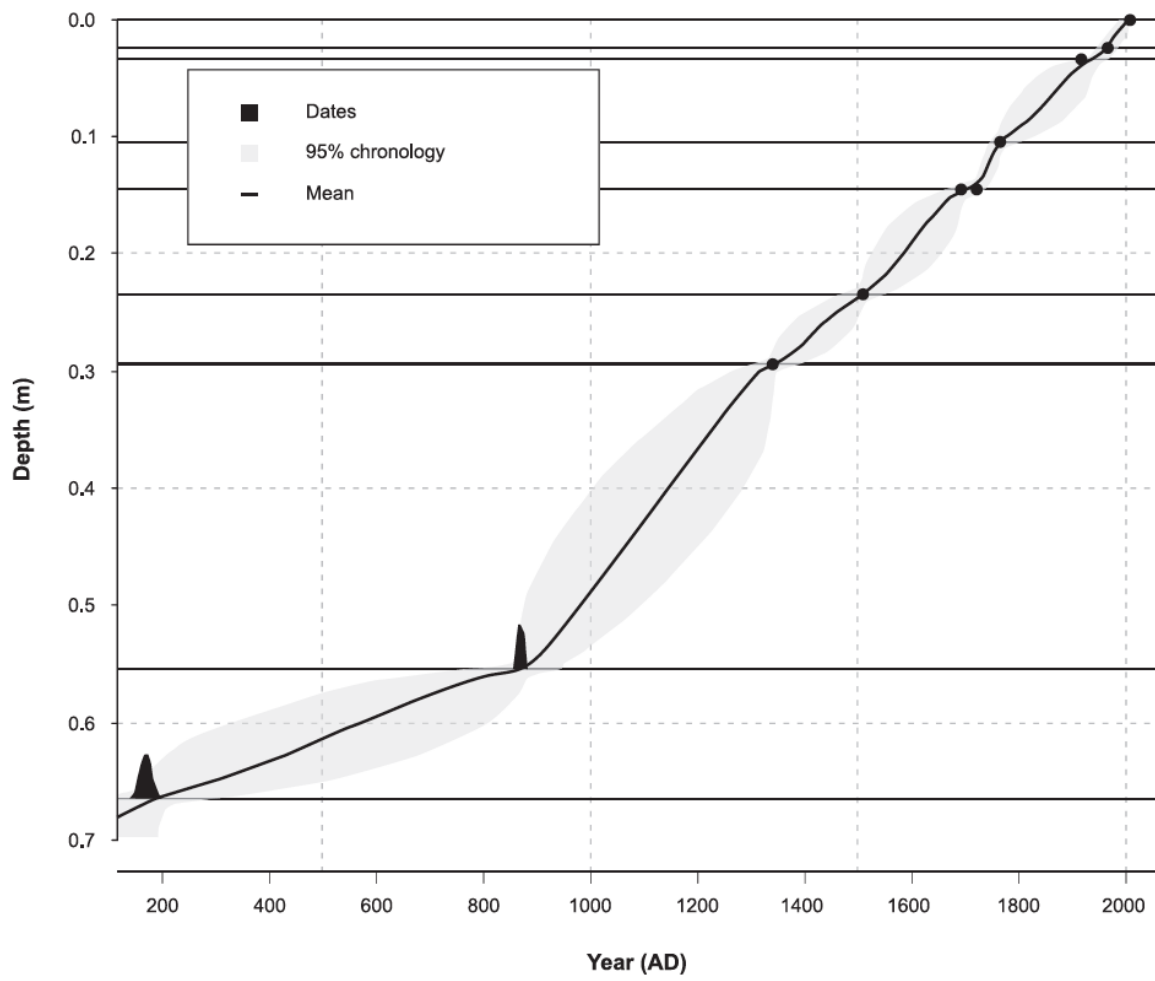


Fig 5

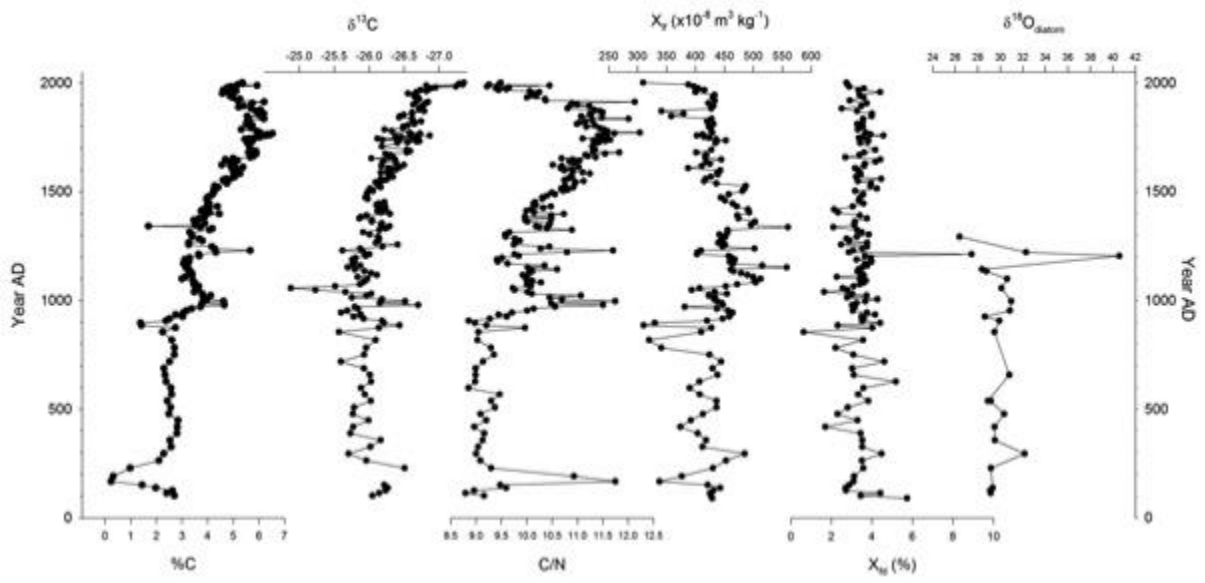


Fig 6

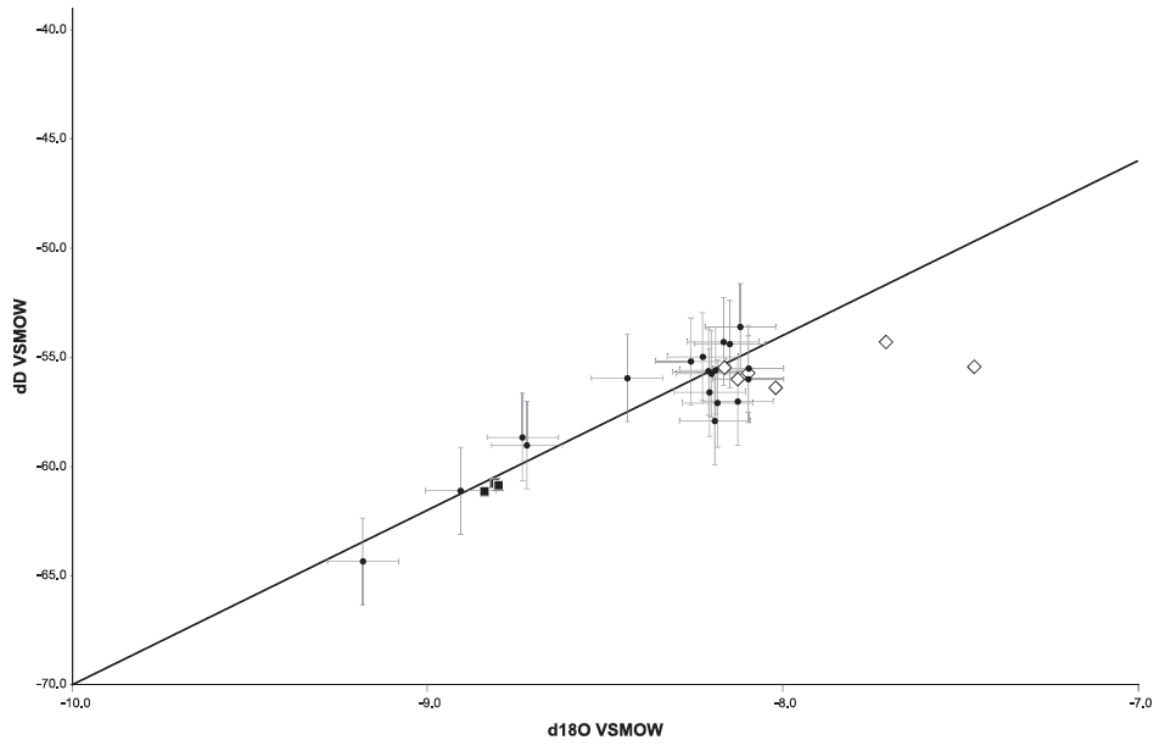


Fig 7

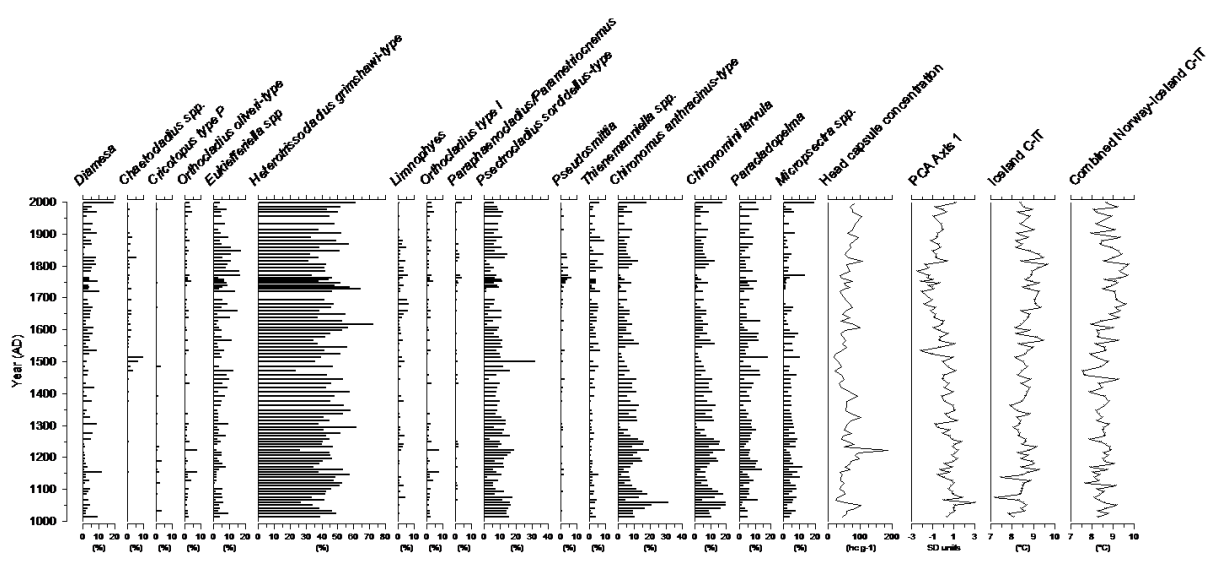


Fig 8

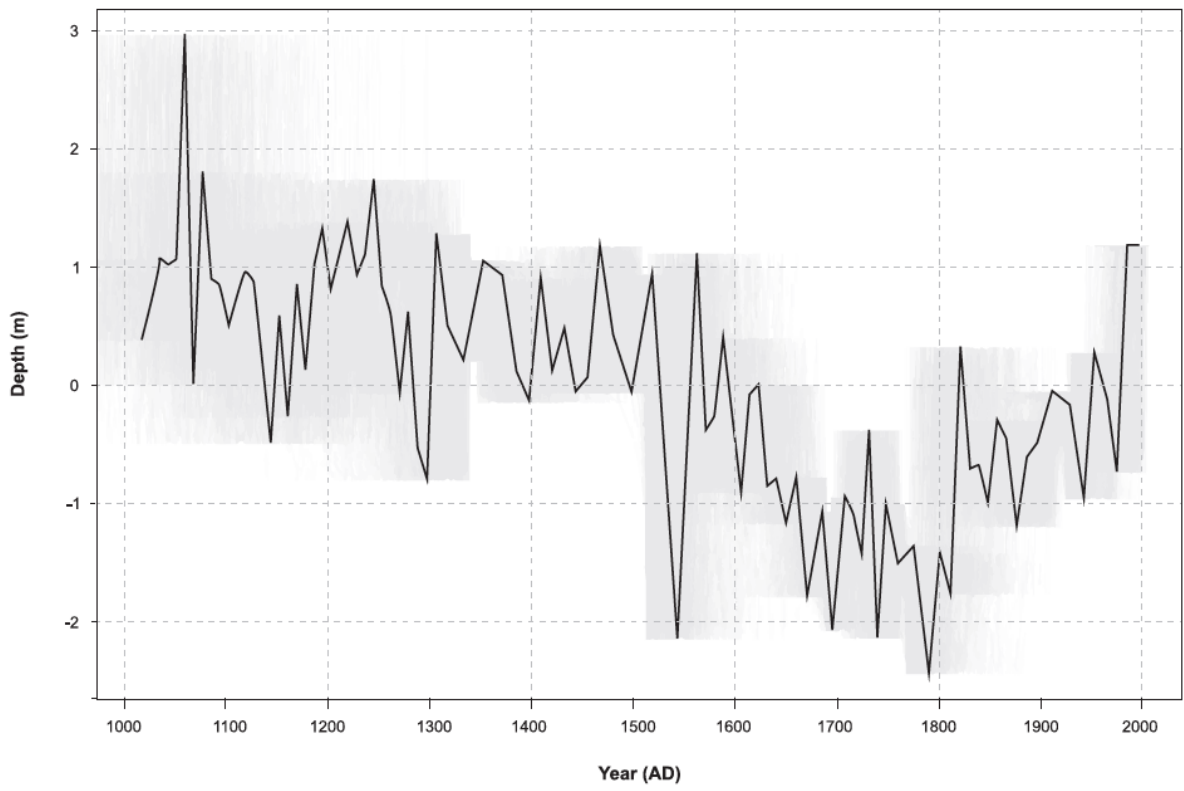


Fig 9

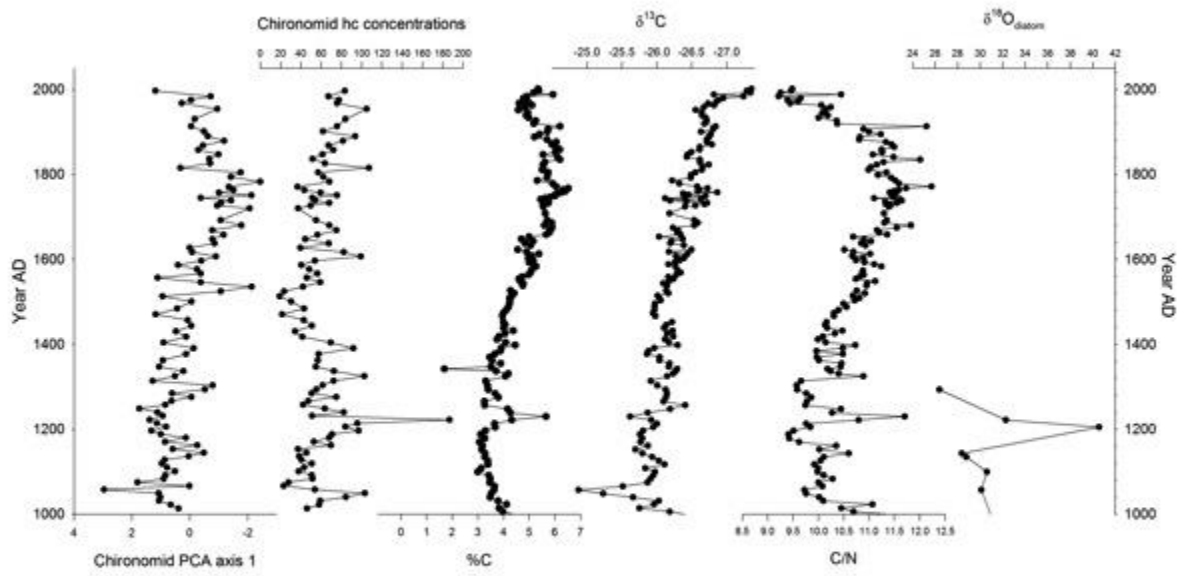


Fig 10

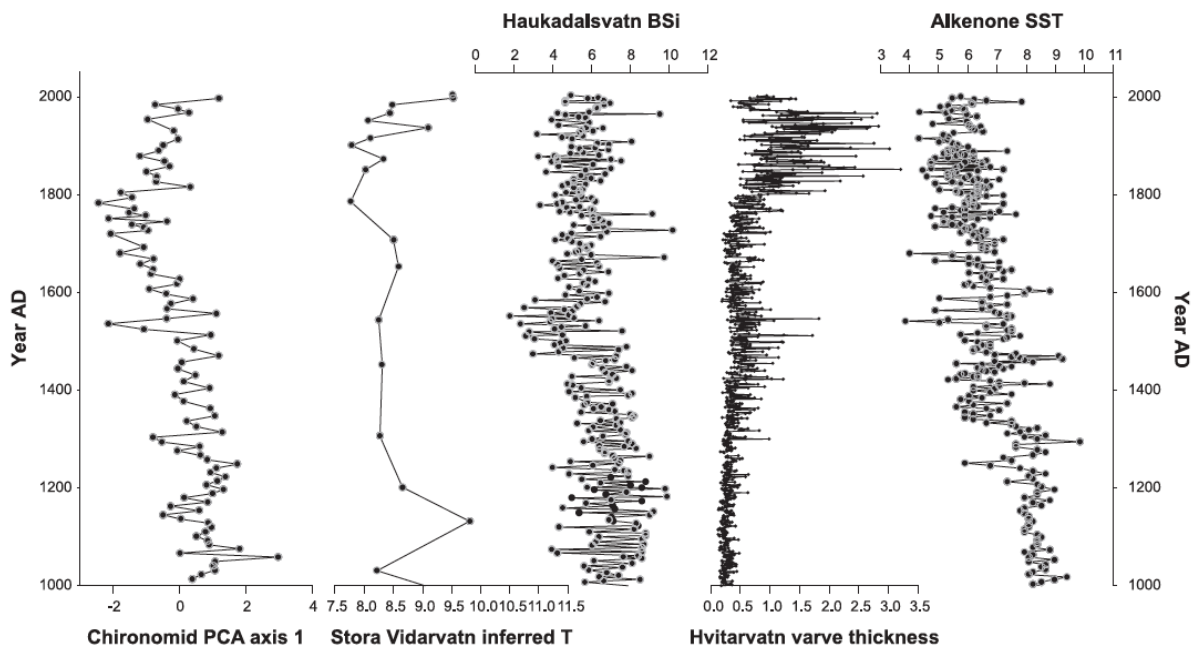


Fig 11

